Electrochimica Acta

Enhancing the Activity of Fe-N-C Oxygen Reduction Reaction Electrocatalysts by High-Throughput Exploration of Synthesis Parameters

--Manuscript Draft--

Manuscript Number:	
Article Type:	VSI: SAE 2022
Keywords:	Iron; Electrocatalyst; Non-PGM; ORR; mass activity; EXAFS
Corresponding Author:	Magali S. Ferrandon Argonne National Laboratory Lemont, UNITED STATES
First Author:	Magali S. Ferrandon
Order of Authors:	Magali S. Ferrandon
	Jaehyung Wang
	Xiaoping Wang
	Eric Coleman
	A. Jeremy Kropf
	Deborah J. Wang
Abstract:	The most active class of platinum group metal-free (PGM-free) oxygen reduction reaction (ORR) electrocatalysts in acidic electrolytes are those synthesized by heat treatment of iron, carbon, nitrogen precursors (Fe-N-C). Due to the large number of possible precursor compounds, a small fraction of the synthesis variable space has been explored. Correlation of synthesis variables with Fe speciation and ORR activity have been limited. In this work, an automation platform and a multi-port ball-milling were utilized to evaluate the effects of synthesis variables, such as identity of iron precursor, iron loading, and carbon and nitrogen sources on the oxygen reduction reaction (ORR) activity of iron-nitrogen-carbon catalysts in acidic electrolyte. The ORR activity is correlated with catalyst Fe speciation determined using Fe K-edge X-ray absorption spectroscopy (XAFS).

Enhancing the Activity of Fe-N-C Oxygen Reduction Reaction Electrocatalysts by High-Throughput Exploration of Synthesis Parameters

Magali S. Ferrandon[a], Jaehyung Park[a], Xiaoping Wang[a], Eric Coleman[b], A. Jeremy Kropf[a] and Deborah J. Myers[a]

a Chemical Sciences and Engineering Division, Argonne National Laboratory, Lemont, IL, 60439, USA

b Materials Science Division, Argonne National Laboratory, Lemont, IL 60439 USA

ABSTRACT

The most active class of platinum group metal-free (PGM-free) oxygen reduction reaction (ORR) electrocatalysts in acidic electrolytes are those synthesized by heat treatment of iron, carbon, nitrogen precursors (Fe-N-C). Due to the large number of possible precursor compounds, a small fraction of the synthesis variable space has been explored. Correlation of synthesis variables with Fe speciation and ORR activity have been limited. In this work, an automation platform and a multi-port ball-milling were utilized to evaluate the effects of synthesis variables, such as identity of iron precursor, iron loading, and carbon and nitrogen sources on the oxygen reduction reaction (ORR) activity of iron-nitrogen-carbon catalysts in acidic electrolyte. The ORR activity is correlated with catalyst Fe speciation determined using Fe K-edge X-ray absorption spectroscopy (XAFS).

Keywords: Iron; Electrocatalyst; Non-PGM; ORR; mass activity; EXAFS

Corresponding author: Magali Ferrandon, ferrandon@anl.gov

1. INTRODUCTION

Polymer electrolyte fuel cells (PEFCs) are electrochemical devices that convert the chemical energy in hydrogen to electrical energy with high efficiency and, as such, are being implemented to eliminate the emission of carbon dioxide from light [1] and heavy-duty vehicles [2]. While light-duty fuel cell electric vehicles were first commercialized in 2014 [3], significant reductions in fuel cell stack cost and hydrogen cost are needed for these vehicles to be cost competitive with the incumbent internal combustion engine-fossil fuel powered vehicles [4,5]. A major contributor to the high cost of PEFC stacks is the high loading of platinum-based electrocatalyst needed to drive the kinetically sluggish oxygen reduction reaction (ORR). An extensive effort has been underway for more than fifty years to replace the platinum-based ORR catalyst with a platinum group metal-free (PGM-free) catalyst comprising earth-abundant materials [6]. Although significant progress has been made over the past decade in increasing both the ORR activity and durability of PGM-free catalysts [7-14], further improvements in these materials, especially in durability and hydrogen-air performance are needed for them to be viable for vehicle power [15]. The highest ORR activities for PGM-free materials have been obtained from catalysts derived from iron salts and metal-organic frameworks or carbon-nitrogen-containing polymers [14-18], though the ORR turnover frequencies and volumetric active site densities of these materials are still approximately one order of magnitude lower than that those of state-of-the-art Pt alloy nanoparticle catalyst [12].

For the general class of pyrolyzed iron-nitrogen-carbon PGM-free materials, variables such as the iron precursor, carbon and nitrogen sources, their relative concentrations, as well as the temperature and atmosphere of pyrolysis are important in determining the activity and stability of the resulting catalysts [13,16,19,20]. Changing the synthesis variable and testing their effect on the resulting catalyst properties, such as iron speciation, and, most importantly, ORR activity, is a

very time-consuming process and only a limited portion of the composition and temperature space have been explored for this broad class of materials [21].

In 2011, Dodelet et al. [16] developed a new synthetic method for Fe-N-C catalysts using physical mixing, through ball milling, of a zeolitic imidazolate framework (ZIF-8), 1,10-phenanthroline, and iron precursors. Ball milling involves high energy movement of beads/milling media which can break chemical bonds, hence, triggering solid–solid reactions, can change the materials' morphology, and possibly forming structural defects that can increase the density of active catalytic sites [22,23]. Unlike liquid phase synthesis of doped ZIFs, high-energy ball milling followed by controlled thermal annealing is an easy and scalable synthetic method in which type of precursors and concentrations can be readily varied [24].

This paper describes a subset of the data from our exploration of the synthesis parameter space of Fe-N-C catalysts derived from ball-milled mixtures of iron salts and carbon and nitrogen-containing compounds. This is aided by the application of high-throughput synthesis methodology to explore the effects of identity of the iron precursor, carbon and nitrogen source, ratio of carbon and nitrogen sources, and iron loading on the activity of iron-based ORR electrocatalysts. Other variables studied and reported upon elsewhere are temperature ramp rate, heat treatment temperature, cooling rate [25] and presence of additional transition metals. A robotic platform and multi-port high-energy ball milling apparatus were utilized to synthesize numerous compositions that were subsequently characterized for ORR activity using aqueous acidic electrolyte rotating ring-disk electrode measurements. The ORR activity is correlated with the Fe speciation determined using Fe K-edge X-ray absorption spectroscopy data.

2. EXPERIMENTAL

2.1 Materials

ZIF-8 (Sigma Aldrich), 1,10-phenanthroline, (abbreviated as phen) (Sigma-Aldrich), and oxidized BP (Black Pearls 2000 pretreated in 70% nitric acid at 80 °C for 8 h) were dried under vacuum for ~15 h at 80 °C. Iron precursors (iron (II) acetate (99.99%, Sigma Aldrich), iron (II) chloride tetrahydrate (98%, Sigma Aldrich), iron (III) chloride anhydrous (99.99%, Sigma Aldrich), iron (III) acetylacetonate (97%, Sigma-Aldrich), iron (III) nitrate nonahydrate (98%, Sigma Aldrich), iron (II) sulphate heptahydrate (>99%, Sigma Aldrich), iron (III) meso-tetra (2,4,6 trimethylphenyl) porphine chloride (Frontier Scientific), ferrocenium tetrafluoroborate (Sigma Aldrich), iron (III) oxalate dihydrate (99%, Sigma-Aldrich), iron (III) meso-tetraphenylporphine μ-oxodimer (Frontier Scientific), 2,3,7,8,12,13,17,18-octaethyl-21h,23h-porphine iron (III) acetate, (97%, Sigma Aldrich), iron (III) phthalocyanine-4,4′,4″,4‴-tetrasulfonic acid, with oxygen monosodium salt hydrate (Sigma Aldrich), 5,10,15,20-tetraphenyl-21h,23h-porphine iron (III) chloride (Sigma Aldrich), iron (III) meso-tetra (4-sulfonatophenyl) porphine chloride (acid form) (Frontier Scientific), iron (III) meso-tetra(4-carboxylphenyl) porphine chloride (Frontier Scientific), 5,10,15,20-tetrakis(pentafluorophenyl)-21h-,23h-porphyrin iron (III) chloride (Sigma Aldrich) and bis(cyclopentadienyl)iron (98%, Sigma Aldrich)) were used as received.

2.2 High-Throughput Catalysis Synthesis

An automated synthesis platform (Big Kahuna, Unchained Labs Inc.) in a custom-built N_2-filled glovebox (MB 200B, MBraun) in Argonne National Laboratory's High-throughput Research Laboratory was used for several steps in the catalyst synthesis. Matrices of experiments and protocols were designed in Library Studio while Automation Studio (LEA software) was used for running the protocols. The solid precursors were dispensed through disposable shaker vials and

weighed using an automated balance (± 0.2 mg accuracy). The synthesis method was inspired by and was similar to the one reported by Zitolo et al. [8]. A mixture of carbon source (Black Pearls) and carbon-nitrogen source (ZIF-8 and phen) and the iron precursor were taken out of the glove box after weighing and placed into 50 mL stainless steel ball mill jars and ball milled at 400 rpm for 2 h in a high-throughput planetary ball mill (PM 400, Retsch). The samples were then heated in a flowing argon atmosphere to 1050 °C, at a heating rate of 5 °C min^{-1}, and held at 1050 °C for 1 h. The sample was then cooled to 900 °C in Ar and exposed to a flowing pure NH_3 atmosphere for 5 min before cooling down naturally to room temperature in Ar.

2.3 Rotating Disk Electrode (RDE)

The ORR half-wave potential ($E_{1/2}$) and the mass activity were evaluated for each catalyst using the thin-film rotating disk electrode (RDE) technique (E7R9 ThinGap RRDE Tips PTFE, Pine Research) and a CHI potentiostat (CH Instruments, Inc.) [26]. Half-wave potential is a valid way to compare ORR activities of catalysts when using the same areal loading of catalyst on the disk electrode [27], but mass activity provides a metric that can be used to compare activities of catalysts evaluated at different loadings and is more useful for translating to the fuel cell performance. The RRDE was immersed in oxygen-saturated room-temperature 0.5 M H_2SO_4 electrolyte also containing a graphite rod counter electrode and Ag/AgCl reference electrode. A catalyst-ionomer ink was prepared by dispersing 5 mg of catalyst in 20 µL of Nafion dispersion (5 wt% Nafion, D521, Ion Power, Inc.) and 0.5 mL of isopropanol. The mixture was sonicated in an ultrasonic ice water bath for 30 min. The catalyst ink was deposited onto the glassy carbon electrode of the RRDE in four aliquots, resulting in a catalyst loading of 0.6 mg cm^{-2}. The Ag/AgCl reference electrode was calibrated versus a platinum electrode in H_2-purged 0.5 M H_2SO_4

electrolyte; all potentials are reported versus this reversible hydrogen electrode (RHE). The catalyst layer was pre-conditioned in cyclic voltametric scans from 0 to 1.0 V at a scan rate of 100 mV/s to remove impurities and ensure fully wetting of the catalyst layer and stable cyclic voltammograms (CVs). The capacitance of selected catalysts, as a relative measure of the surface area of the catalysts exposed to the electrolyte, was calculated using the double layer charging current region with potentials ranging from 0.1 to 0.4 V. Steady-state ORR polarization curves were recorded in oxygen-saturated 0.5 M H_2SO_4 electrolyte using staircase voltammetry from 1.0 to 0 V with a potential step of 20 mV and a step period of 20 sec. The rotation rate of the RRDE was 900 rpm.

2.4 Catalyst Characterization

2.4.1 X-ray absorption spectroscopy

X-ray absorption spectroscopy (XAFS) measurements at the Fe *K*-edge were carried out in either transmission or fluorescence mode at the 10-ID and 10-BM beam lines at Argonne National Laboratory's Advance Photon Source. The near-edge regions of the XAFS spectra (7105 to 7155 eV) were fit using the linear combination algorithm of the *Athena* software (version 0.8.054), based on the *IFEFFIT* code [28], to the spectra for two Fe-containing standards: an oxygen adduct of Iron(III) phthalocyanine-4,4´,4´´,4´´´-tetrasulfonic acid (Fe(III)pc) and iron carbide (Fe_3C). Fe(III)pc is a widely-used standard for the first-shell coordination environment of the Fe species typically observed in this class of catalysts and Fe in a first shell coordination environment similar to that of Fe(III)pc or its pyridinic rather than pyrrolic analog have been proposed to be the associated with the active site [8]. The Fe_3C was chosen as the other primary component of the

synthesized materials based on the presence of characteristic features of Fe_3C in the k-space representation and Fourier transform of the extended regions of the XAFS spectra.

2.4.2 Inductively coupled plasma optical emission spectroscopy (ICP-OES)

The weight loading of Fe in these catalyst samples were analyzed utilizing elemental analyses by ICP-OES performed by Galbraith Laboratories.

3. RESULTS AND DISCUSSION

3.1 Effect of Carbon Source

Black pearls carbon (BP) was used as the carbon source for the Fe-N-C catalysts as it has a high surface area and high electronic conductivity [29]. The weight percentage of phen with respect to the total weight of phen and BP was varied between 0 and 75 wt.% phen, while keeping the content of iron acetate constant (0.5 wt.% Fe with respect to total weight of precursors before heat treatment). Phen content higher than 75 wt.% (with respect to the weight of phen plus BP) resulted in heat treated powders that could not be dispersed into a usable ink for the evaluation of ORR activity. The Fourier transforms of the iron *K*-edge EXAFS data for the materials obtained after heat treatment and for the model compounds (Fe(III)pc and Fe_3C) are plotted in Fig. 1A. At phen contents between 25 and 60 wt.%, the Fourier transforms are similar to that of Fe(III)pc suggesting that the majority Fe in the samples is in a local coordination environment similar to that of Fe(III)pc (i.e., FeN_4O_x). The concentration of N-coordinated pyridinic or pyrrolic Fe sites has been experimentally correlated with ORR activity and these sites have been modeled to be the most active ORR active sites in Fe-based catalysts [8,30-36]. Iron carbide species, when encapsulated

by N-doped carbon, have also been reported to be ORR active, however, FeN_x sites have been reported to be more active for the four-electron reduction and to produce less peroxide [37]. As noted in the Fourier transforms of the EXAFS data, there is a clear shift of the first shell Fe−N/O bond length observed in the catalysts compared to that in the structurally well-defined Fe(III)pc [38]. According to Li et al., the shortening of the Fe−N bond leads to changes in electronic structure, such as positive shifting of the 3d-orbitals of central Fe and a larger charge transfer from Fe to adjacent N facilitating oxygen adsorption on the FeN_4 sites [38]. Linear combination fitting (LCF) of the XANES data for the catalysts to that of the Fe_3C and Fe(III)pc standards (Fig. 1B) shows that the catalyst derived from precursor contains a mixture of Fe in coordination environments similar to the two standards. When there is no phen in the initial mixture (i.e., no nitrogen source in the precursors), the molar ratio of Fe(III)pc-like species determined from LCF is 0.4, with nitrogen presumably derived from the ammonia treatment [16]. However, the ammonia treatment alone is not enough to provide a high FeN_x content. The mole fraction of Fe in FeN_4O_x coordination increases linearly with the concentration of the nitrogen-containing precursor up to 40 wt.% phen and plateaus between 40 and 50 wt.% phen. With increasing phen content, the mole fraction of Fe(III)pc-like coordination increases to 0.74 at 50 wt.% phen. At higher phen contents, the Fe(III)pc-like coordination decreases until reaching a mole fraction of 0.4 at 75 wt.% phen. The ORR mass activity at 0.8 V correlates with the fraction of Fe in FeN_4O_x coordination between 25 and 60 wt.% phen, with a maximum ORR activity of 1.8 A/g ($E_{1/2}$ = 0.75 V) at 50 wt.% phen. When the initial concentration of phen is increased, there are various phenomena that might occur simultaneously that explain the observed correlations. Phen, which contains N, contributes to the increased formation of N-containing species while at the same time, during pyrolysis, loss of carbon from the mixture will be higher when compared to the more thermally stable BP-rich

samples. This leads to an increase in both the fraction of Fe in FeN_4O_x sites and the final total iron content with increasing phen content. One can speculate that at higher concentrations of phen, above 50 wt.%, there is a loss of both carbon and nitrogen, such that the overall iron content is higher than the N content necessary to form the FeN_x sites and thus iron carbide is formed. It can also be speculated that with increasing phen there is less carbon to stabilized FeN_x sites in the graphene plane and hence more iron carbide prevails.

When ZIF-8 is used (instead of BP), species with FeN_4O_x coordination are observed predominantly in all samples from 0 to 75 wt.% phen (Fig. 2A), as determined from the Fourier transform of the EXAFS data. At phen contents higher than 50 wt.%, the powders obtained after pyrolysis were not dispersible in ionomer-solvent inks for RRDE ORR activity evaluation, therefore characterization was not performed on these materials. The mole fractions of Fe in FeN_4O_x and Fe_3C-like coordination and the ORR mass activity are plotted as a function of the phen wt.% (relative to the weight of phen plus ZIF-8) in Fig. 2B. In the absence of phen, the initial mole fraction of FeN_4O_x species is 0.8. This molar fraction remains constant up to 10% phen, decreases at higher phen contents, then increases again to 40% phen. The initial decrease in FeN_x with increasing phen is most likely due to the lower N content in phen (16 wt.%) versus that of ZIF-8 (25 wt.%). When comparing BP- vs ZIF-based syntheses (Fig.1B vs 2B), ZIF clearly leads to a higher mole fraction of FeN_4O_x species (maximum of 0.8 mole fraction versus 0.74). This is certainly due to the additional nitrogen provided by ZIF-8 compared to the carbon-only BP. The ORR mass activity shows a complex dependence on phen to ZIF-8 ratio and a complex relationship with FeN_4O_x content, which was not observed in the case of the phen/BP system. By combining two precursors that are undergoing major structural and chemical changes during heat treatment,

one might expect synergetic or antagonist effects also dependent on the ratio of these two precursors to the Fe content in the precursors. In addition, the presence of Fe_3C might boost the ORR activity of nearby FeN_4 [39] such that the ultimate ORR activity of the material depends not only on the absolute FeN_4 content, but on the proximity of Fe_3C to the FeN_4 sites. The highest ORR activity was obtained at 40 wt. % phen, as was the case with the phen/BP system, with an ORR mass activity of 8.6 A/g and a $E_{½}$ of 0.809 V, which is also the catalyst with the highest mole fraction of FeN_4O_x. Proietti *et al.* studied the effect of phen content (0 to 75 wt. % versus ZIF-8) and reported the highest fuel cell (tested in H_2-O_2) power density for a catalyst prepared using 20 wt.% phen, but found that the catalyst activity was independent of the phen content except for 0 and 75 wt.% [16].

3.2 Effect of Fe loading

Using the phen and ZIF-8 contents resulting in the highest ORR mass activity and $E_{1/2}$ in the 0.5 wt.% Fe study described above (40 and 60 wt.%, respectively), the loading of iron (II) acetate in the precursors was varied to give an Fe content from 0 to 1.0 wt.%. Fig. 3A shows the Fourier transform of the EXAFS data. The final Fe loading in the catalyst and the mass activity as a function of the initial Fe loading in the precursor are shown in Fig. 3B, while the speciation is shown in Fig. 3C. Increasing the Fe content in the precursors up to 0.70 wt.% leads to an increase in both the total Fe content and the Fe-N_x content in the catalyst (2.12 wt.% in the final catalyst) and a decrease at precursor Fe contents > 0.70 wt.%. The loading of Fe_3C was found to increase monotonically with increasing Fe precursor content (Fig. 3C). According to Li et al., only a limited number of ultra-fine FeO_x clusters formed during the heat treatment of Fe precursors can transform into atomically-dispersed Fe-N_x, likely limited by the number of N-containing vacancies in the

carbon structure formed during heat treatment of ZIF-8 [38]. Excess Fe can react with the abundant carbon in the system to form carbide. Iron is also known to enhance graphitization, which explains the increase of Fe_3C with Fe concentration in the precursor [40,41]. The highest ORR activity, 9.45 A/g, was observed with 0.8 wt.% Fe in the precursor (1.90 wt.% Fe in the catalyst) with a $E_{½}$ of 0.816 eV, which is substantially higher than the previously-reported ORR mass activity of 2.8 A/g for this class of materials [42].

3.3 Effect of Fe precursors

The ORR mass activities at 0.8V for catalysts derived from twelve different Fe precursors (in addition to Fe acetate) are shown in Table 1 with the optimized composition (40 : 60 weight ratio of phenanthroline to ZIF-8 and 0.8 wt.% Fe of the mixture phen-ZIF). The iron precursors were chosen because they contain porphyrin or phthalocyanine structure-like. The catalyst derived from the precursor mixture containing iron acetate was found to be by far the most active, followed by iron acetylacetonate. All other catalysts were substantially less active than the iron acetate-derived catalyst. A plot of ORR mass activity versus electrochemical capacitance for the catalysts derived from the different iron precursors indicates that the ORR mass activity may be correlated with catalyst surface area, with the exception of the catalyst derived from the iron acetate precursor (Fig. 4). There are apparently additional effects of iron acetate on the physicochemical properties of the resulting catalyst that are beneficial to the catalyst's ORR activity needing further exploration.

Table 1. Mass activity at 0.8V for catalysts derived from various iron precursors (40 : 60 weight ratio of phenanthroline to ZIF-8 and 0.8 wt.% Fe of the mixture phen-ZIF).

Iron Precursors	Mass activity (A/g)
Iron (II) acetate	9.45
Iron (III) acetylacetonate	4.41
Iron (III) meso-tetra (2,4,6 trimethyl phenyl) porphine chloride	3.13
Ferrocenium tetrafluoroborate	3.95
Iron (II) oxalate dihydrate	4.81
Iron (III) meso-tetraphenylporphine u-oxodimer	3.99
2,3,7,8,12,13,17,18-octaethyl-21h,23h-porphine iron (III) acetate	4.07
Iron (III) phthalocyanine-4,4′,4″,4‴-tetrasulfonic acid	2.52
5,10,15,20-tetraphenyl-21h,23h-porphine iron (III) chloride	3.01
Iron (III) meso-tetra (4-sulfonatophenyl) porphine chloride (acid form)	2.03
Iron (III) meso-tetra(4-carboxylphenyl) porphine chloride	1.22
5,10,15,20-tetrakis(pentafluorophenyl)-21h-,23h-porphyrin iron (III) chloride	0.99
Bis(cyclopentadienyl)iron	4.51

The short-term stability of the catalyst synthesized using the optimized conditions determined in this study was evaluated by measuring successive ORR traces, as shown in Fig. 5. There is an initial loss of 6 mV after the second potential cycle, but no additional losses were observed in the third potential cycle.

4. CONCLUSIONS

This work evaluated the synthesis variables of identity of iron precursor, iron loading, and carbon and nitrogen source content (black pearls carbon, phenanthroline, and ZIF-8) on the ORR activity in acidic electrolyte of Fe-N-C catalysts obtained after heat treatment of the precursor mixture. The ORR activities determined using the thin-film RDE technique are correlated with Fe speciation in the catalysts determined using Fe K-edge X-ray absorption spectroscopy (XAFS). The major findings of this work are:

- Increasing phenanthroline content in the ball-milled mixture of Fe, phenanthroline, and BP carbon precursor promotes formation of species with Fe phthalocyanine-like first shell coordination (FeN_4O_x) at intermediate concentrations and formation of Fe carbide at high concentrations, with the ORR mass activity correlated with FeN_4O_x content;
- Use of ZIF-8 versus the black pearls-phenanthroline source of carbon and nitrogen promotes formation of species with FeN_4O_x first shell coordination;
- The weight percentage of species with FeN_4O_x first shell coordination increases linearly with increasing Fe content in the precursor up to 0.5 wt.% and reached the maximum at 0.8 wt.% then decreases at higher Fe contents. A decrease in total Fe content and formation of Fe carbide are responsible for this limitation to the maximum content of Fe species with FeN_4O_x first shell coordination;
- When using different Fe-N-C compounds as the source of Fe, the different Fe compounds resulted in different catalyst electrochemical surface area, as evidenced by changes in the double layer capacitance, and ORR activity was correlated with the surface area with the exception of the catalyst derived from iron acetate;
- The maximum ORR activity observed in this study of Fe-N-C catalysts derived from ball-milled iron salt, nitrogen, carbon precursors was observed for a catalyst synthesized using

60 wt.% ZIF, 40 wt.% phenanthroline and 0.8 wt.% Fe in the precursor and iron acetate as the Fe source.

ACKNOWLEDGMENTS

The authors would like to thank Ulises Martinez from Los Alamos National Laboratory for providing oxidized Black Pearls. This work was supported by the U.S. Department of Energy, Energy Efficiency and Renewable Energy, Hydrogen and Fuel Cell Technologies Office under the auspices of the Electrocatalysis Consortium (ElectroCat). This research used the resources of the Advanced Photon Source (APS), a U.S. Department of Energy (DOE) Office of Science User Facility operated for the DOE Office of Science by Argonne National Laboratory under Contract No. DE-AC02-06CH11357. Argonne National Laboratory is managed for the U.S Department of Energy by the University of Chicago Argonne, LLC, also under contract DE-AC-02-06CH11357. XAFS data were acquired at MRCAT at the APS. MRCAT operations are supported by the Department of Energy and the MRCAT member institutions.

REFERENCES

[1] Y. Wang, H. Yuan, A. Martinez, P. Hong, H. Xu, F.R. Bockmiller, Polymer electrolyte membrane fuel cell and hydrogen station networks for automobiles: Status, technology, and perspectives, Adv. Appl. Ener. 2 (2021) 100011.

[2] D.A. Cullen, K.C. Neyerlin, R.K. Ahluwalia, R. Mukundan, K.L. More, R.L. Borup, A.Z. Weber, D.J. Myers, A. Kusoglu, New roads and challenges for fuel cells in heavy-duty transportation, Nature Energy, 6 (2021) 462.

[3] T. Yoshida, K. Kojima, Toyota MIRAI fuel cell vehicle and progress toward a future hydrogen society, Electrochem. Soc. Interface, 571 (2015) 24.

[4] B. James, J. Huya-Kouadio, C. Houchins, D. Desantis, Mass Production Cost Estimation of Direct H2 PEM Fuel Cell Systems for Transportation Applications: 2018 Update, Final SA 2018 Transportation Fuel Cell Cost Analysis -2020-01-23. DOI: 10.13140/RG.2.2.12165.99049.

[5] S.T. Thompson, B.D. James, J.M. Huya-Kouadio, C. Houchins, D.A. Desantis, R. Ahluwalia, A.R. Wilson, G. Kleen, D. Papageorgopoulos, Direct hydrogen fuel cell electric vehicle cost analysis: System and high-volume manufacturing description, validation, and outlook, J. Power Sources, 399 (2018) 304.

[6] Y. He, G. Wu, PGM-Free Oxygen-Reduction Catalyst Development for Proton-Exchange Membrane Fuel Cells: Challenges, Solutions, and Promises, Acc. Mater. Res. 3 (2022) 224.

[7] M. Lefèvre, E. Proietti, F. Jaouen, and J.-P. Dodelet, Iron-based catalysts with improved oxygen reduction activity in polymer electrolyte fuel cells, Science, 324 (2009) 71.

[8] A. Zitolo, V. Goellner, A. Armel, M.-T. Sougrati, T. Mineva, L. Stievano, E. Fonda, F. Jaouen, Identification of catalytic sites for oxygen reduction in iron- and nitrogen-doped graphene materials, Nature Mater. 14 (2015) 937.

[9] M. Shao, Q. Chang, J.-P. Dodelet, R. Chenitz, Recent advances in electrocatalysts for oxygen reduction reaction, Chem. Rev. 116 (2016) 3594.

[10] H. Zhang, S. Hwang, M. Wang, Z. Feng, S. Karakalos, L. Luo, Z. Qiao, X. Xie, C. Wang, D. Su, Y. Shao, G. Wu, Single atomic iron catalysts for oxygen reduction in acidic media: particle size control and thermal activation, J. Am. Chem. Soc. 139 (2017) 14143.

[11] Y. Chen, S. Ji, C. Chen, Q. Peng, D. Wang, Y. Li, Single atom catalysts: synthetic strategies and electrochemical applications, Joule 2 (2018) 1242.

[12] F. Jaouen, D. Jones, N. Coutard, V. Artero, P. Strasser, A. Kucernak, Toward platinum group metal-free catalysts for hydrogen/air proton-exchange membrane fuel cells, Johnson Matthey Technol. Rev., 62(2) (2018) 231.

[13] X. Wan, X. Liu, Y. Li, R. Yu, L. Zheng, W. Yan, H. Wang, M. Xu, J. Shui, Fe−N−C electrocatalyst with dense active sites and efficient mass transport for high-performance proton exchange membrane fuel cells, Nat. Catal. 2 (2019) 259.

[14] C. Wan, X. Duan, Y. Huang, Molecular design of single-atom catalysts for oxygen reduction reaction, Adv. Energy Mater. 10 (2020) 1903815.

[15] L. Osmieri, J. Park, D.A. Cullen, P. Zelenay, D.J. Myers, K. C. Neyerlin, Status and Challenges for the Application of Platinum Group Metal-Free Catalysts in Proton Exchange Membrane Fuel Cells, Current Opinion in Electrochemistry, 25 (2021) 100627.

[16] E. Proietti, F. Jaouen, M. Lefèvre, N. Larouche, J. Tian, J. Herranz, and J.-P. Dodelet, Iron-based cathode catalyst with enhanced power density in polymer electrolyte membrane fuel cells, Nature Comm. 416 (2011) 1.

[17] H. Zhang, H. Osgood, X. Xie, Y. Shao, and G. Wu, Engineering nanostructures of PGM-free oxygen-reduction catalysts using metal-organic frameworks, Nano Energy 31 (2017) 331.

[18] X. Tian, X.F. Lu, B.Y. Xia, X. W. Lou, Advanced electrocatalysts for the oxygen reduction reaction in energy conversion technologies, Joule 4, (2020) 45.

[19] V. Armel, S. Hindocha, F. Salles, S. Bennett, D. Jones, Structural descriptors of zeolitic−imidazolate frameworks are keys to the activity of Fe−N−C catalysts, J. Am. Chem. Soc. 139 (2017) 453.

[20] M. Chen, Y. He, J.S. Spendelow, G. Wu, Atomically dispersed metal catalysts for oxygen reduction, ACS Energy Lett. 4 (2019) 1619.

[21] M.K. Jeon, C.H. Lee, G. Il Park, K.H. Kang, Combinatorial search for oxygen reduction reaction electrocatalysts: A review, J. Power Sources 216 (2012) 400.

[22] T. Xing, J. Sunarso, W. Yang, Y. Yin, A.M. Glushenkov, L. Hua Li, P.C. Howlettb, and Y. Chen, Ball milling: a green mechanochemical approach for synthesis of nitrogen doped carbon nanoparticles, Nanoscale 5 (2013) 7970.

[23] A. Shen, Y. Zou, Q. Wang, R.A.W. Dryfe, X. Huang, S. Dou, L. Dai, S. Wang, Oxygen reduction reaction in a droplet on graphite: direct evidence that the edge is more active than the basal plane, Angew. Chem. Int. Ed. 53 (2014) 10804.

[24] X. Chen, L. Yu, S. Wang, D. Deng, X. Bao, Highly active and stable single iron site confined in graphene nanosheets for oxygen reduction reaction, Nanoenergy 32 (2017) 353.

[25] W.J.M. Kort-Kamp, M. Ferrandon, X. Wang, J. Hyung Park, R.K. Malla, T. Ahmed, E.F. Holby, D.J. Myers, Piotr Zelenay, Adaptive Learning-Driven High-throughput Synthesis of Oxygen Reduction Reaction Fe-N-C Electrocatalysts, accepted J. Power Sources.

[26] T.J. Schmidt, H.A. Gasteiger, G.D. Stäb, P.M. Urban, D.M. KoIb, R.J. Behm, Characterization of high-surface-area electrocatalysts using a rotating disk electrode configuration, J. Electrochem. Soc 145(7) (1998) 2354.

[27] D.E. Beltrán, S. Litster, Half-wave potential or mass activity? Characterizing platinum group metal-free fuel cell catalysts by rotating disk electrodes, ACS Energy Letters 4(5) (2019) 1158.

[28] B. Ravel and M. Newville, ATHENA, ARTEMIS, HEPHAESTUS: data analysis for X-ray absorption spectroscopy using IFEFFIT, J. Synchrotron Rad. 12 (2005) 537.

[29] A. Macías-García, M.A. Díaz-Díez, M. Alfaro-Domínguez, J.P. Carrasco-Amador, Influence of chemical composition, porosity and fractal dimension on the electrical conductivity of carbon blacks, Heliyon 6(6) (2020) e04024.

[30] U.I. Koslowski, I. Abs-Wurmbach, S. Fiechter, P. Bogdanoff, Nature of the catalytic centers of porphyrin-based electrocatalysts for the ORR: A correlation of kinetic current density with the site density of Fe-N4 centers, J. Phys. Chem C 112 (2008) 15356.

[31] F. Calle-Valejo, J. Ignacio Martínez, J. Rossmeisl, Density functional studies of functionalized graphitic materials with late transition metals for oxygen reduction reactions, Phys. Chem. Chem. Phys. 13 (2011) 15639.

[32] H.T. Chung, D.A. Cullen, D. Higgins, B.T. Sneed, E.F. Holby, K.L. More, P. Zelenay, Direct atomic-level insight into the active sites of a high-performance PGM-free ORR catalyst, Science 357 (2017) 479.

[33] H. Xu, D. Cheng, D. Cao, X.C. Zeng, A universal principle for a rational design of single-atom electrocatalysts, Nat. Catal. 1 (2018) 339.

[34] A. Gewirth, J.A. Varnell, A. M. DiAscro, Nonprecious metal catalysts for oxygen reduction in heterogeneous aqueous systems, Chem. Rev. 118 (2018) 2313.

[35] L. Yang, D. Cheng, H. Xu, X. Zeng, X. Wan, J. Shui, Z. Xiang, D. Cao, Unveiling the high-activity origin of single-atom iron catalysts for oxygen reduction reaction, PNAS 115(26) (2018) 6626.

[36] E.F. Holby, P. Zelenay, Linking structure to function: The search for active sites in non-platinum group metal oxygen reduction reaction catalysts, Nanoenergy 29 (2016) 54.

[37] S.SA. Shah, T. Najam, C. Cheng, L. Peng, R. Xiang, L. Zhang, J. Deng, W. Ding, Z. Wei, Exploring Fe-Nx for peroxide Reduction: template-free synthesis of Fe-Nx traumatized mesoporous carbon nanotubes as an ORR catalyst in acidic and alkaline solutions, Chem. Eur. J. 24 (2018) 10630.

[38] J. Li, H. Zhang, W. Samarakoon, W. Shan, D.A. Cullen, S. Karakalos, M. Chen, D. Gu, K.L. More, G. Wang, Z. Feng, Z. Wang, G. Wu, Thermally driven structure and performance evolution of atomically dispersed FeN4 sites for oxygen reduction, Angew. Chem. Int. Ed. 58 (2019) 18971.

[39] W.-J. Jiang, L. Gu, L. Li, Y. Zhang, X. Zhang, L.-J. Zhang, J.-Q. Wang, J.-S. Hu, Z. Wei, L.-J. Wan, Understanding the high activity of Fe−N−C electrocatalysts in oxygen reduction: Fe/Fe3C nanoparticles boost the activity of Fe−Nx, J. Am. Chem. Soc. 138 (2016) 3570.

[40] H. Marsh, A.P. Warburton, Catalysis of Graphitization, J. Appl. Chem. 20 (1970) 133.

[41] U.I. Kramm, I. Herrmann-Geppert, S. Fiechter, G. Zehl, I. Zizak, I. Dorbandt, D. Schmei□er, P. Bogdanoff, Effect of iron-carbide formation on the number of active sites in Fe–N–C catalysts for the oxygen reduction reaction in acidic media, J. Mater. Chem. A 2 (2014) 2663.

[42] M. Primbs, Y. Sun, A. Roy, D. Malko, A. Mehmood, M.-T. Sougrati, P.Y. Blanchard, G/ Granozzi, T. Kosmala, G. Daniel, P. Atanassov, J. Sharman, C. Durante, A. Kucernak, D. Jones, F. Jaouen, P. Strasser, Establishing reactivity descriptors for platinum group metal (PGM)-free Fe-N-C catalysts for PEM fuel cells, Energy Environ. Sci 13 (2020) 2480.

List of Figures

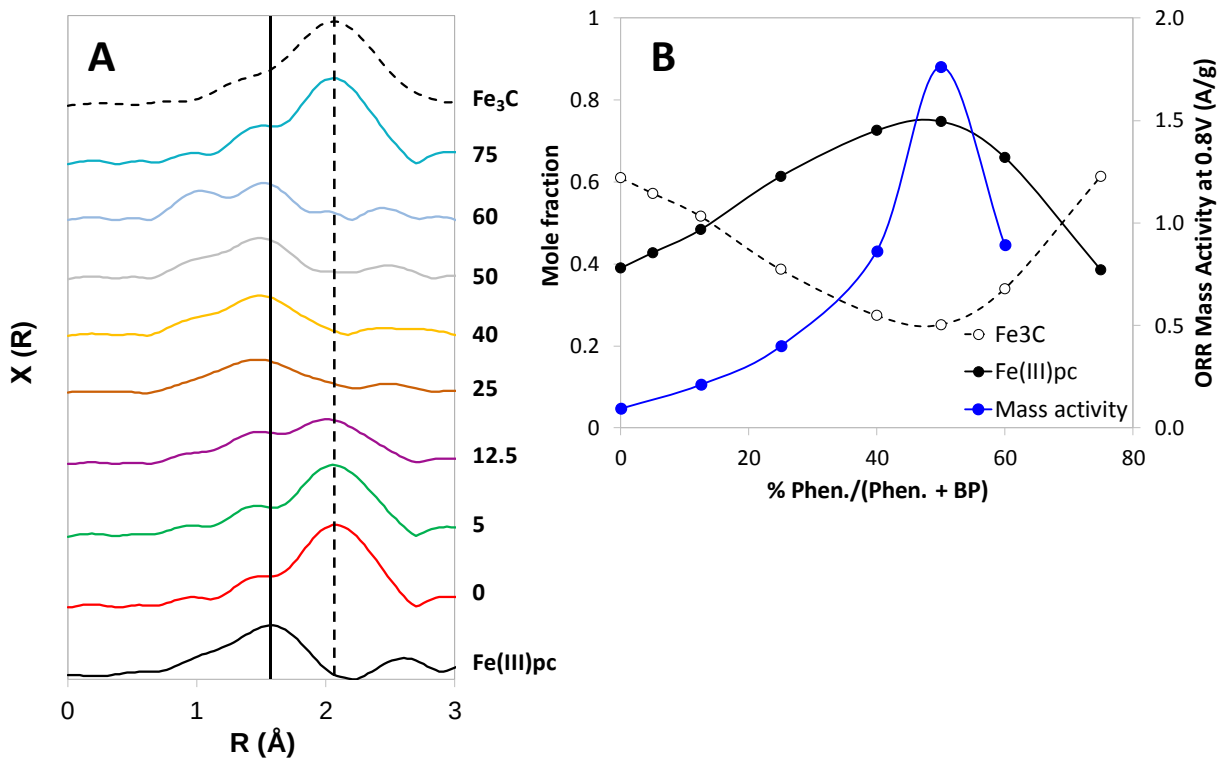

Fig. 1. Fourier transforms of the Fe K-edge EXAFS data as a function of 1,10-phenanthroline loading (wt.%) in the initial mixture of phenanthroline and BP (not phase corrected, Fe(III)pc and Fe_3C data shown for comparison) (A) mole fraction of Fe_3C-like and Fe(III)pc-like coordination, determined by XANES LCF, and ORR mass activity at 0.8V as a function of 1,10-phenanthroline loading (initial target loading of 0.5 wt.% Fe using iron (II) acetate) (B).

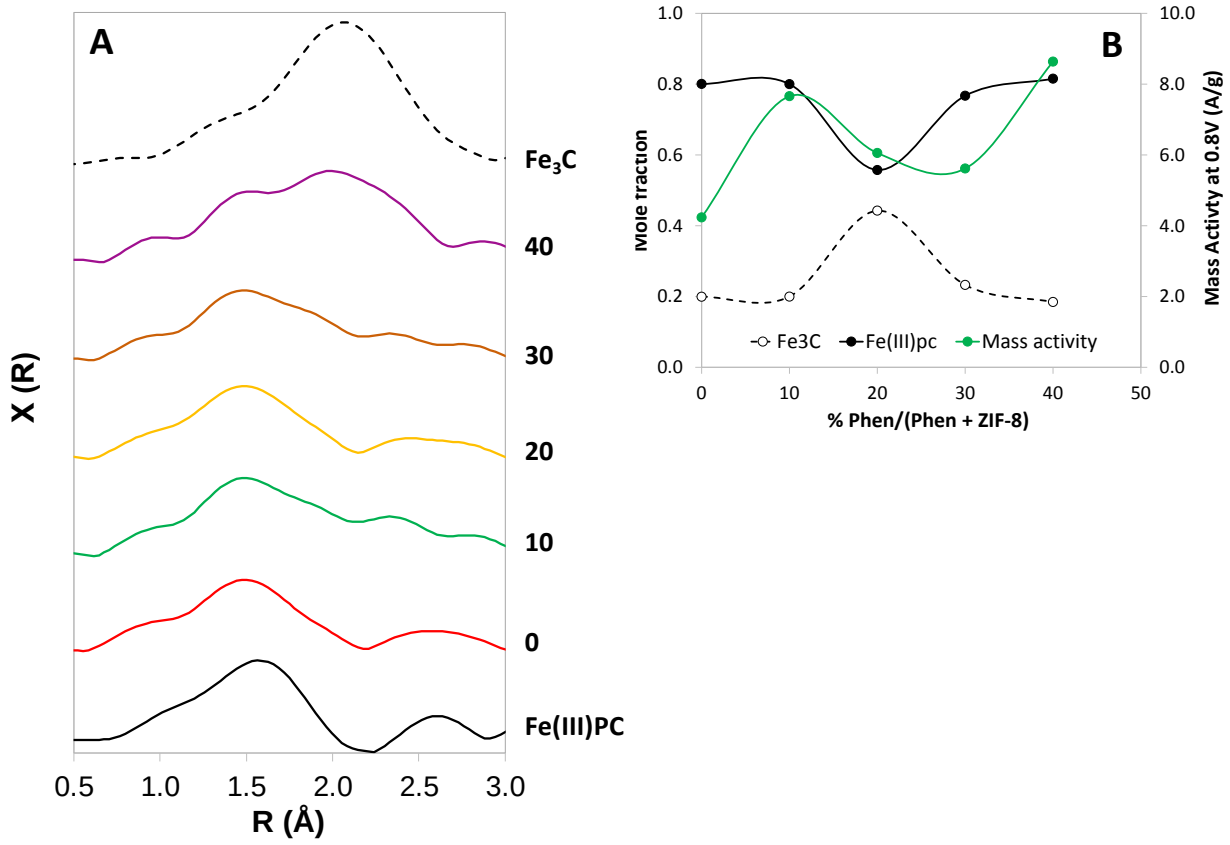

Fig. 2. Fourier transform of Fe K-edge EXAFS data (not phase corrected) as a function of 1,10-phenanthroline loading (wt.%) in the initial mixture of 1,10-phenanthroline and ZIF-8; data for Fe(III)pc and Fe_3C standards shown for comparison) (A), mole fraction of Fe_3C-like and Fe(III)pc-like coordination determined by LCF, and ORR mass activity at 0.8V as a function of 1,10-phenanthroline loading (initial target loading of 0.5 wt.% Fe using iron (II) acetate) (B).

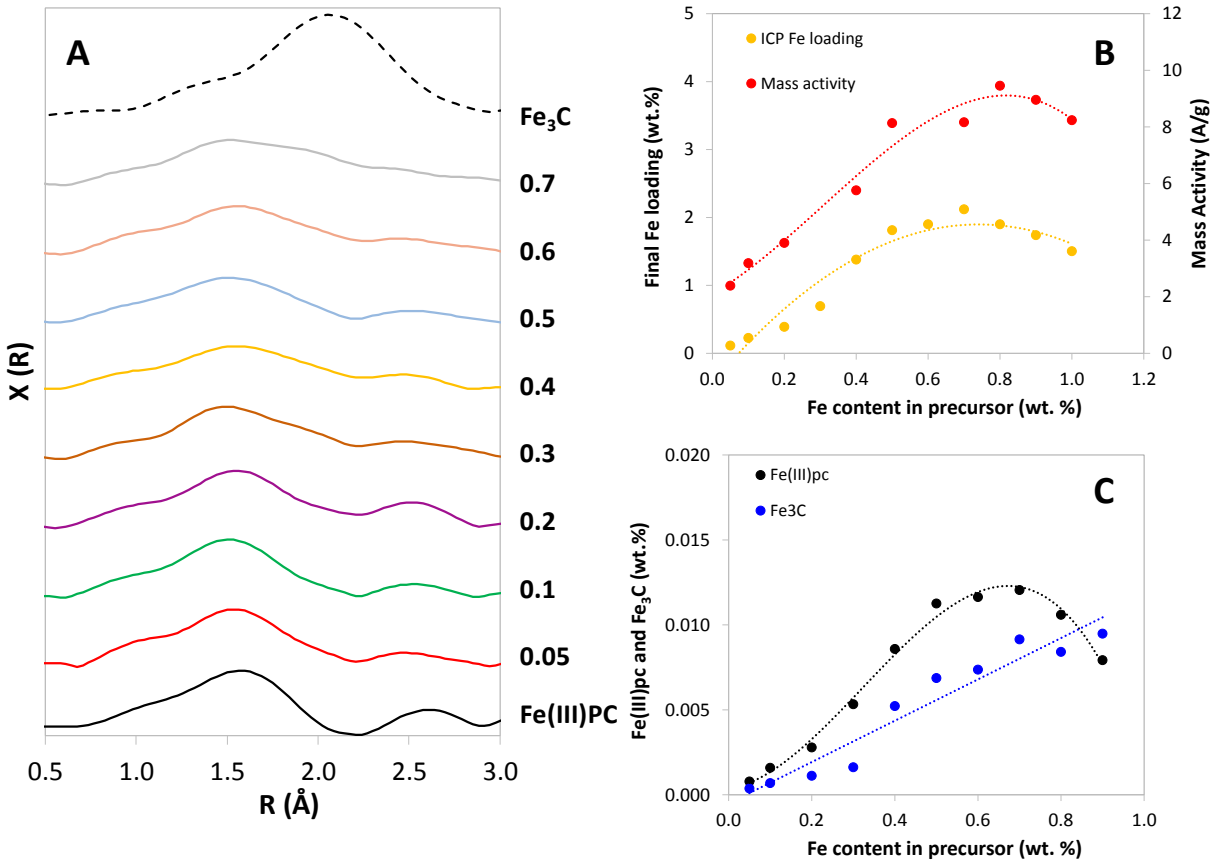

Fig. 3. Fourier transform of Fe K-edge EXAFS data (not phase corrected) as a function of Fe content (wt.%) in the initial mixture of 1,10-phenanthroline and ZIF-8; Fe(III)pc and Fe_3C standard data shown for comparison (A), actual Fe loading determined by ICP and mass activity at 0.8 V (B), Fe(III)pc and Fe_3C loading (wt.%) determined by XANES LCF (C), at 40 wt.% 1,10-phenanthroline and 60 wt.% ZIF-8 (iron (II) acetate used as precursor).

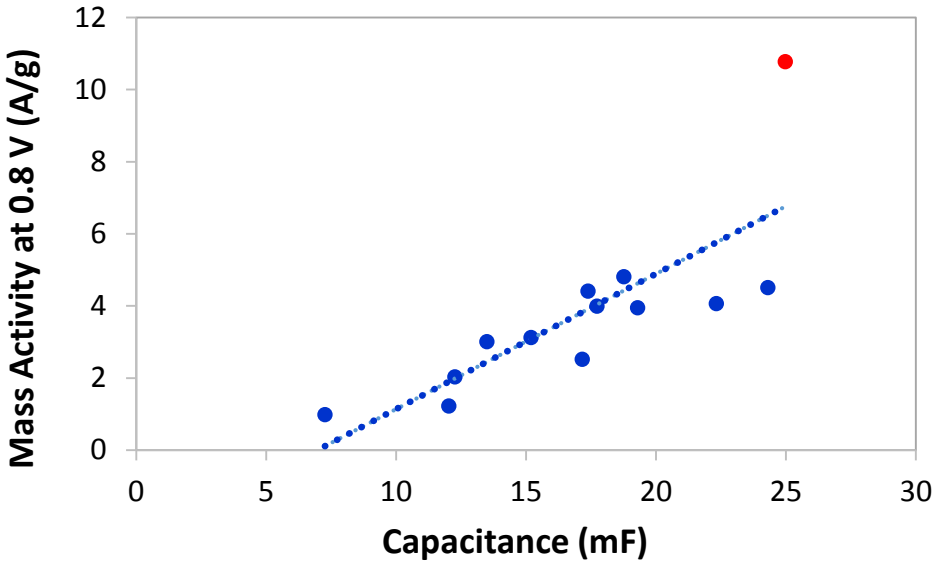

Fig. 4. Mass activity as a function of capacitance for all the catalysts using various Fe precursors from Table 1 in blue dots (except using iron acetate, red dot).

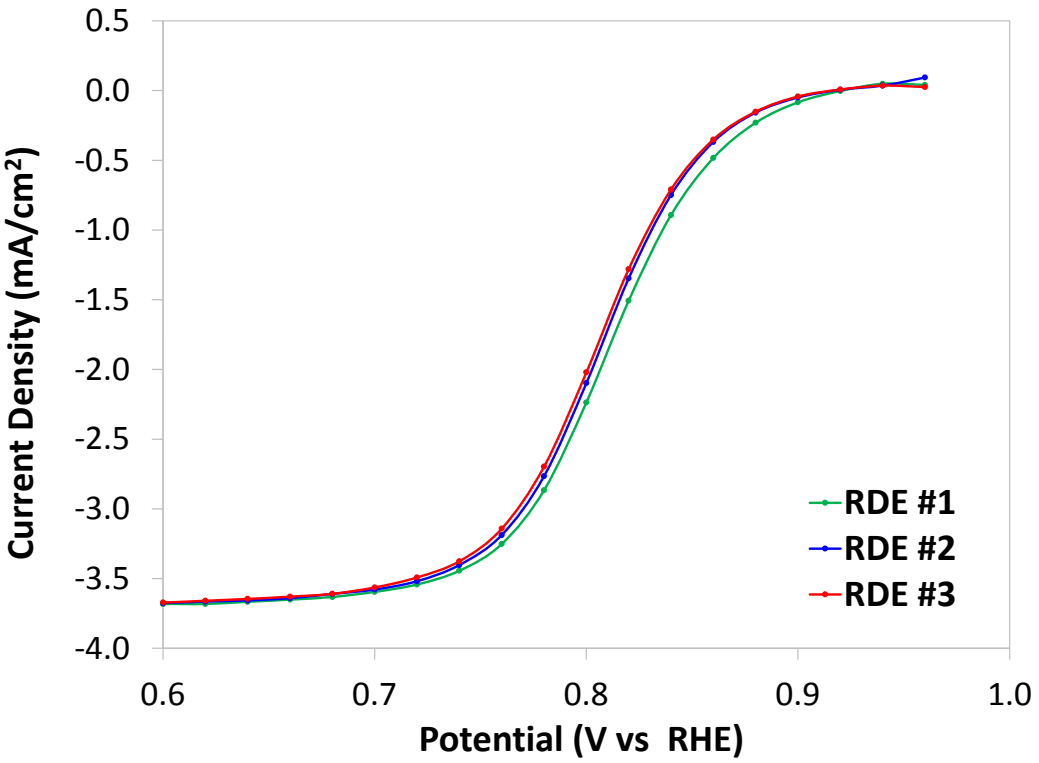

Fig. 5. First, second, and third ORR potential sweeps for the Fe-N-C catalyst derived from precursors with 0.8 wt.% (iron (II) acetate), 40 wt.% 1,10-phenanthroline, and 60 wt.% ZIF-8. Conditions: 0.6 mg-cat/cm^2, 900 rpm, O_2-saturated 0.5 M H_2SO_4.

Subject: Manuscript Submission to Special Issue of Electrochimica Acta

Dear Editor,

Please find enclosed our manuscript entitled "*Enhancing the Activity of Fe-N-C Oxygen Reduction Reaction Electrocatalysts by High-Throughput Exploration of Synthesis Parameters*" by Magali S. Ferrandon, Jaehyung Park, Xiaoping Wang, Eric Coleman, A. Jeremy Kropf, and Deborah J. Myers. This paper is in response to your recent message to Dr. Deborah Myers inviting us to submit our work to the special issue on the themed collection on "Single Atom Electrocatalysts".

In our manuscript, an automation platform and a multi-port ball-milling were utilized to evaluate the effects of synthesis variables, such as identity of iron precursor, iron loading, and carbon and nitrogen sources (black pearls carbon, phenanthroline, and ZIF-8) and content on the oxygen reduction reaction (ORR) activity of iron-nitrogen-carbon (Fe-N-C) catalysts in acidic electrolyte. The ORR activities in acidic electrolyte, determined using the thin-film RDE technique, are correlated with Fe speciation in the catalysts determined using Fe K-edge X-ray absorption spectroscopy (XAFS). In summary, in our exploration of the synthesis variables in this class of synthetic procedure for single-atom Fe-N-C ORR catalysts, we obtained the highest ORR activity using 60 wt.% ZIF, 40 wt.% phenanthroline and 0.8 wt.% Fe in the precursor mixture and iron acetate as the Fe source. The ORR activity obtained in our study was greater than three times that reported in the literature for this synthesis method. The ORR activity was correlated with the concentration of Fe in an FeN_4O_x first shell coordination environment, as determined by linear combination fitting of the near-edge region of the XAFS spectra.

We are looking forward to receiving your comments and suggestions.

Sincerely,

Magali Ferrandon, on behalf of all the co-authors.

Declaration of interests

☒The authors declare that they have no known competing financial interests or personal relationships that could have appeared to influence the work reported in this paper.

☐The authors declare the following financial interests/personal relationships which may be considered as potential competing interests: